Article

Copyright © 2014 American Scientific Publishers
All rights reserved
Printed in the United States of America

Journal of
Nanoscience and Nanotechnology
Vol. 14, 9632–9636, 2014
www.aspbs.com/jnn

Surface Modification and Characterization of Electrosprayed Sn-Doped In_2O_3 Thin Films

Bon-Ryul Koo and Hyo-Jin Ahn*

Department of Materials Science and Engineering, Seoul National University of Science and Technology, Seoul 139-743, South Korea

We synthesized Sn-doped In_2O_3 (Indium tin oxide, ITO) thin films using electrospray and spin-coating. Scanning electron microscopy, atomic force spectroscopy, X-ray diffraction, X-ray photoelectron spectroscopy, Hall-effect measurement, and UV-vis spectrophotometry measurements were performed to investigate the morphological, structural, chemical, electrical, and optical properties of the electrosprayed ITO films with a sol-layer coating for surface modification. To obtain the optimum performance of the resultant ITO thin films after surface modification, we heat-treated them at four different temperatures of 450 °C (sample A), 550 °C (sample B), 650 °C (sample C), and 750 °C (sample D) using microwave heating. Surface modified ITO thin films calcined at 550 °C (sample B) using electrospray and spin-coating are observed to have superior resistivity (9.9×10^{-3} $\Omega \cdot$cm) and optical transmittance (~92.08%) owing to the improved densification of the ITO surface by spin-coating and the formation of uniform ITO thin films by electrospraying.

Delivered by Publishing Technology to: Sung Kyun Kwan University
Copyright: American Scientific Publishers

Keywords: Sn-Doped In_2O_3, TCO, Electrospray, Spin-Coating, Microwave Heating.

1. INTRODUCTION

Indium tin oxide (ITO, Sn-doped In_2O_3) thin films, which are indispensable in various applications such as electrochromic devices, organic photovoltaic devices, organic light-emitting devices, photocatalysis, and NO_2 sensor, are the preferred transparent conductive oxides (TCO).[1–5] ITO has advantages such as a low resistivity ($1–3 \times 10^{-4}$ $\Omega \cdot$cm) and high optical transmittance (80–83%). To date, various synthetic methods to obtain high-quality ITO thin films have been developed, mainly through two different approaches. One approach involves vacuum-based processes that include magnetron sputtering, E-beam evaporation, and chemical vapour deposition (CVD),[6–8] which are used for the commercial production of ITO thin films despite high production costs. The other approach involves solution-based processes that include spray pyrolysis, inkjet-printing, and spin coating.[9–11] For example, Moholkar et al. have synthesized ITO thin films using spray pyrolysis and investigated their structural, electrical, and optical properties as a function of precursor concentration parameters. Thus, ITO thin films have been obtained with a resistivity of $\sim 2.71 \times 10^{-3}$ $\Omega \cdot$cm and transmittance of ~94.4%.[9] Hwang et al. reported inkjet-printing of ITO films for use as TCOs with an observed resistivity of $\sim 3 \times 10^{-2}$ $\Omega \cdot$cm and transmittance of ~87% after annealing at 400 °C.[10] Ting et al. used a sol–gel spin-coating method with different indium precursor solutions synthesized from $In(NO_3)_3$ or $InCl_3$. The indium nitrate-derived ITO thin films exhibited resistivity and transmittance of $\sim 4.2 \times 10^{-3}$ $\Omega \cdot$cm and ~85%, respectively.[11] As these examples show, the development trends of TCOs are recently changing from vacuum-based processes to solution-based processes. In particular, the challenge of developing a novel synthetic method for solution-based TCO thin films is a very important issue. We recently introduced an electrospray technique for fabricating solution-based ITO thin films. Till date, the electrospray technique has been used mostly in applications such as electrospray ionization (ESI), thin-film deposition, and colloidal thrusters because electrospray has advantages such as low cost, simplicity, and deposition feasibility for large area films in a non-vacuum atmosphere.[12]

In this study, we successfully fabricated solution-based ITO thin films using electrospray and then introduced spin-coating for surface modification to improve the performance of the ITO thin films.

*Author to whom correspondence should be addressed.

 1533-4880/2014/14/9632/005 doi:10.1166/jnn.2014.10150

2. EXPERIMENTAL DETAILS

ITO thin films were successfully synthesized on glass substrates (Corning EAGLE XG™) using electrospray and spin-coating as follows. For electrospraying, indium chloride tetrahydrate ($InCl_3 \cdot 4H_2O$, Aldrich) and tin chloride dihydrate ($SnCl_2 \cdot 2H_2O$, Aldrich), used as starting materials, were dissolved in 2-propanol for 3 h. The molar ratio of In:Sn precursors to fabricate an optimum ITO solution was fixed at 9:1. A typical electrospraying apparatus consists of a syringe pump with a plastic syringe, a collector, and a high-voltage power supply. The feeding rate is fixed at 0.02 mL/h and the distance between the needle tip and the collector is maintained at ~10 cm under a high voltage of 24 kV. The optimum deposition of ITO nanoparticles on the substrates occurs for a deposition time of 15 min at 80% chamber humidity. The as-deposited ITO thin films were dried at 150 °C in an oven for 3 h and then heat-treated at four different calcination temperatures of 450 °C, 550 °C, 650 °C, and 750 °C (referred to here as sample A before sol-layer coating, sample B before sol-layer coating, Sample C before sol-layer coating, and Sample D before sol-layer coating) using a microwave furnace for 3 h in air. We employed a microwave furnace because of its unique properties such as the reduction of diffusion impurities and damages as well as larger grain size of the ITO nanoparticles in the TCO films due to the rapid heating/cooling, compared to a conventional furnace. In addition, to improve the performance of the electrosprayed ITO thin films, we employed a spin-coating method on these thin films. Using spin-coating, an ITO sol-layer is deposited on the electrosprayed ITO thin films at a speed of 2000 rpm for 30 s using the above-mentioned ITO sol-solution. The resultant ITO thin films are heat-treated again at 450 °C, 550 °C, 650 °C, and 750 °C (referred to here as sample A, sample B, Sample C, and Sample D).

The surface morphology and surface topography of the samples were characterized by field-emission scanning electron microscopy (FE-SEM, Hitachi S-4700) and atomic force microscopy (AFM, XE-100). X-ray diffraction (XRD, Rigaku X-ray diffractometer equipped with a Cu Kα radiation) and X-ray photoelectron spectroscopy (XPS, ESCALAB 250 equipped with an Al Kα X-ray source) were performed to investigate the structural and chemical properties of the samples. The electrical properties including the resistivity, hall mobility, and carrier concentration are characterized by means of a Hall Effect Measurement System (Ecopia, HMS-3000). The transmittance spectra in the wavelength range of 300 nm to 900 nm were measured using a UV-vis spectrophotometer (Scinco, S-3100).

3. RESULTS AND DISCUSSION

Figure 1 shows the top-view FESEM images obtained from samples A, B, C, and D. As the calcination temperature is increased, the size of grains on the ITO thin film is

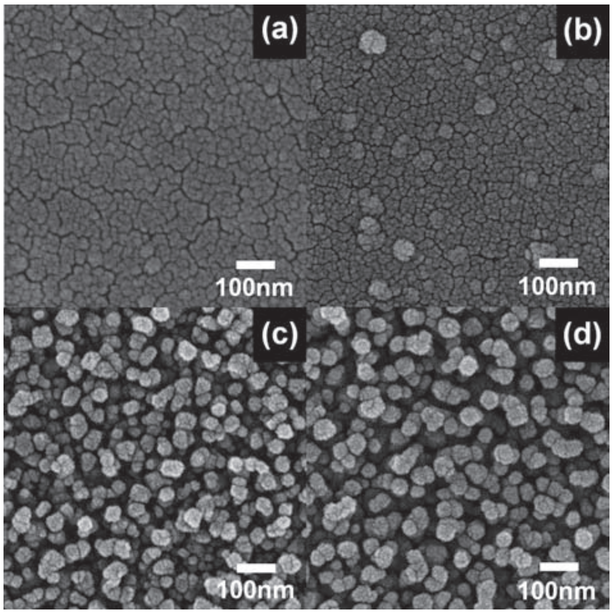

Figure 1. FESEM images obtained from samples A, B, C, and D fabricated using electrospray and spin-coating.

gradually increased. In particular, samples A and B exhibit a uniform surface morphology, which is due to the sol-layer coating deposited by spin-coating and the formation of small-sized grains by calcination at temperatures below 550 °C. In contrast, samples C and D exhibit a rough surface morphology, resulting in a performance drop of the TCOs. Among various performance parameters such as crystallinity, doping content, thickness of the films, and densification, in general, good electrical performance of the TCOs is directly related to the dense surface morphology on the films.[13–16] Thus, samples C and D are considered to have poor electrical properties because of the rough surface morphology and are discussed later. In addition, from the cross-section views of the samples (not shown in here), the thicknesses of the films are observed to be in the range of ~227 nm to ~237 nm for sample A, ~232 nm to 244 nm for sample B, ~247 nm to ~254 nm for sample C, and ~273 nm to 295 nm for sample D. Thus, samples C and D indicate that the thickness of the films increased as the annealing temperature using microwave increased. That is, in case of box and tube furnaces, the thickness of the films is slightly decreased because of enough time for high densification of the films as the annealing temperature increased. However, for the case of microwave annealing, high densification of the films does not occur due to high energy and short reaction time (holding time of 5 min) in high annealing temperatures (i.e., samples C and D). In addition, for samples C and D, the larger grain growth of the ITO films due to high energy and short reaction time occurs, resulting in the rough surface morphology on the ITO films.

Figures 2(a) and (b), which present the AFM images for sample B before and after sol-layer coating, respectively,

Delivered by Publishing Technology to: Sung Kyun Kwan University
IP: 115.145.125.155 On: Wed, 01 Oct 2014 02:23:2
Copyright: American Scientific Publishers

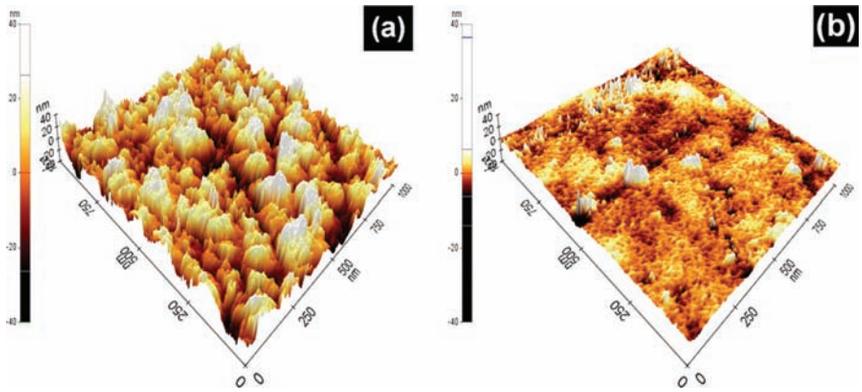

Figure 2. AFM images of (a) sample B before sol-layer coating and (b) sample B after sol-layer coating.

examine the effect of surface modification on the ITO thin films. The average surface roughness was ~10.8 nm for sample B before sol-layer coating and ~2.1 nm for sample B after sol-layer coating. Electrosprayed ITO thin films after sol-layer coating are observed to have dramatically decreased surface roughness when compared to electrosprayed ITO thin films before sol-layer coating. Although sample B before sol-layer coating shows larger irregular grains, sample B after sol-layer coating formed a dense morphology due to the filling of the gaps between the grains by the ITO sol-solution. Thus, the results indicate potential enhancement of electrical properties such as Hall mobility in the electrosprayed and spin-coated ITO thin films.

Figure 3 shows the XRD plots obtained from samples A, B, C, and D after calcination using microwave heating. Broad peaks around 23° correspond to a glass substrate (Corning EAGLE XG™) having an amorphous characteristic. Main diffraction peaks of all the samples are observed at 30.60°, 35.51°, and 51.07°, corresponding to the (222), (400), and (440) planes, respectively. This implies that all the samples possess a polycrystalline phase with cubic bixbyite structure of In_2O_3 (space group la3 [206]; JCPDS card No. 06-0416). In particular, the diffraction peaks observed are slightly shifted toward higher 2θ angle compared to pure In_2O_3. The reference bulk reflections of pure In_2O_3 phases correspond to 30.57°, 35.46°, and 51.03° for the (222), (400), and (440) planes. The results imply that Sn ion substitutes an indium ion in the In_2O_3 lattice since the ionic radius of Sn^{4+} (0.069 nm) is smaller than that of In^{3+} (0.08 nm), which causes a donation of free electrons that improves the conductivity.[17, 18] This result can be explained by using Bragg's equation ($n\lambda = 2d \sin\theta$). Thus, XRD results indicate that Sn ions are doped in the In_2O_3 matrix, implying the successful formation of the ITO thin films using electrospray and spin-coating.

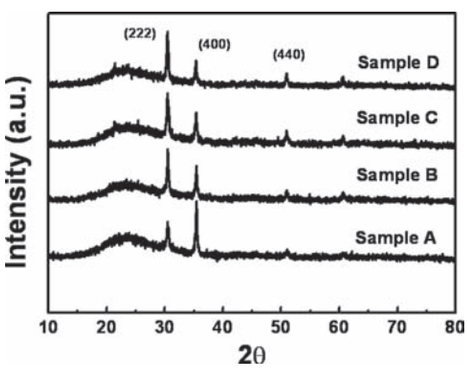

Figure 3. XRD data obtained from samples A, B, C, and D.

To investigate the chemical bonding states of sample B, XPS measurements were carried out, as shown in Figure 4. The photoelectron peaks of In 3*d* and Sn 3*d* are obtained after the calibration of the C 1*s* line (284.5 eV). The In $3d_{5/2}$ and In $3d_{3/2}$ photoelectrons (Fig. 4(a)) of sample B are observed at binding energies of ~444.35 eV and ~451.90 eV, implying that In_2O_3 phases are formed. In addition, the Sn $3d_{5/2}$ and Sn $3d_{3/2}$ photoelectrons (Fig. 4(b)) are observed at binding energies of ~486.20 eV and ~494.60 eV, implying that SnO_2 phases are formed.[19] The O 1*s* photoelectron for sample B is divided into two signals as shown in Figure 4(c). The two signals observed at ~529.80 eV and ~531.2 eV correspond to the chemical bonding between O 1s and In, and O 1s and Sn, respectively. Thus, XPS results indicate that the ITO thin films are composed of In_2O_3 and SnO_2 phases.

Figure 5(a) shows the electrical properties including carrier concentration, hall mobility, and resistivity of samples A, B, C, and D. The carrier concentrations gradually increase from sample A (6.61×10^{19} cm^{-3}) to sample D (9.11×10^{19} cm^{-3}) because of the enhanced crystallinity due to the increasing calcination temperature. The Hall mobilities observed are 9.06 $cm^2/(Vs)$, 9.31 $cm^2/(Vs)$, 5.10 $cm^2/(Vs)$, and 1.55 $cm^2/(Vs)$ for samples A, B, C, and D, respectively. Sample B shows the highest Hall mobility because of the formation of a uniform surface on the ITO thin films. On the other hand, sample D has the lowest value of Hall mobility because

Copyright: American Scientific Publishers

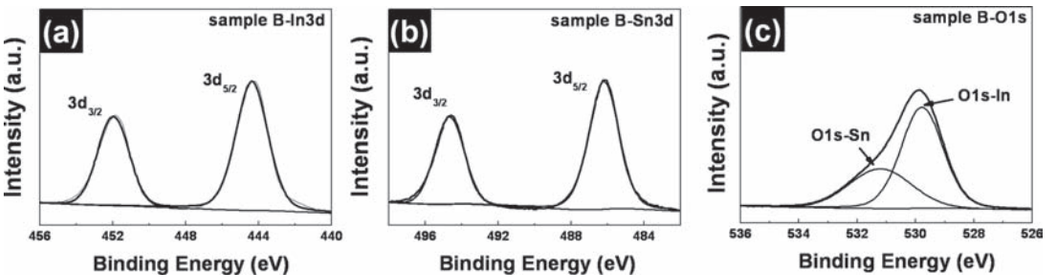

Figure 4. XPS core-level spectra for the In 3*d*, Sn 3*d*, and O 1*s* obtained from sample B.

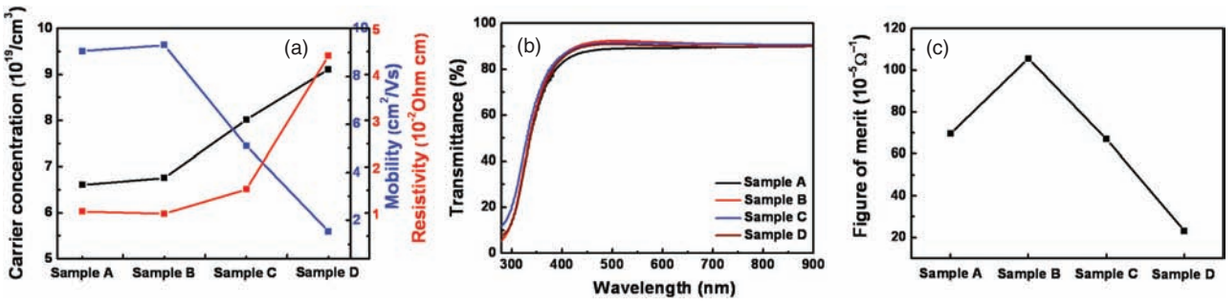

Figure 5. (a) Electrical properties including carrier concentration, Hall mobility, and resistivity, (b) optical transmission spectra, and (c) figure of merit (FOM) obtained from all samples.

of a rough surface on the ITO thin films, as shown in the FESEM images in Figures 1(b) and (d). In addition, to calculate the resistivity (ρ), we can use the following equation:[20]

$$\rho = 1/(Ne\mu)$$

where N is the carrier concentration, e is the electron charge (1.602×10^{-19} C), and μ is the Hall mobility. The values of the resistivity (ρ) thus calculated are $\sim 1.04 \times 10^{-2}$ $\Omega \cdot$cm for sample A, $\sim 9.90 \times 10^{-3}$ $\Omega \cdot$cm for sample B, $\sim 1.52 \times 10^{-2}$ $\Omega \cdot$cm for sample C, and $\sim 4.41 \times 10^{-2}$ $\Omega \cdot$cm for sample D. As can be seen, sample B shows superior resistivity compared to the other samples. The improved densification of the ITO surface due to the sol-layer coating on the electrosprayed ITO thin films is a possible reason for this behaviour. Furthermore, the carrier concentration and Hall mobility for samples A, B, C, and D before the sol-layer coating exhibit relatively low values: 1.93×10^{19} cm^{-3}, 2.24×10^{19} cm^{-3}, 3.96×10^{19} cm^{-3}, and 6.09×10^{19} cm^{-3} and 4.38 cm^2/(Vs), 5.77 cm^2/(Vs), 2.34 cm^2/(Vs), and 1.38 cm^2/(Vs), respectively. Thus, the introduction of the sol-layer coating plays a key role on the performance improvement of the electrosprayed ITO thin films. Figure 5(b) shows the optical transmission spectra obtained from samples A, B, C, and D in the wavelength range of $\sim$300 nm to 900 nm. The transmittances, which are observed at 550 nm, are $\sim$89.09%, $\sim$92.08%, $\sim$91.36%, and $\sim$90.52% for samples A, B, C, and D, respectively. That is, all the samples exhibit similar and excellent transmittances because of the formation of uniform and dense ITO thin films having thicknesses in the range of $\sim$230 nm to $\sim$277 nm. The results, including electrical and optical properties, are summarized in Table I. Finally, to confirm the performance of the TCO films, Figure of Merit (FOM) using the transmittance (T) and sheet resistance (Rs) is calculated using the following equation as shown in Figure 5(c):[21, 22]

$$FOM = T^{10}/Rs$$

The values of FOM are 69.7×10^{-5} Ω^{-1}, 105.6×10^{-5} Ω^{-1}, 67.0×10^{-5} Ω^{-1}, and 23.2×10^{-5} Ω^{-1} for samples A, B, C, and D, respectively, implying that sample B possesses the best performance for use as TCO thin films compared to the other samples.

Table I. Summary of electrical and optical properties for all samples.

samples	Carrier concentration (cm^{-3})	Hall mobility (cm^2/(v·s))	Resistivity ($\Omega \cdot$cm)	Transmittance (%)
Sample A	6.61×10^{19}	9.06	1.04×10^{-2}	89.09
Sample B	6.76×10^{19}	9.31	9.90×10^{-3}	92.08
Sample C	8.02×10^{19}	5.10	1.52×10^{-2}	91.36
Sample D	9.11×10^{19}	1.55	4.41×10^{-2}	90.52

4. CONCLUSION

ITO thin films were successfully fabricated using electrospray and spin-coating. Their surface morphology, structure, chemical states, electrical, and optical properties were investigated by means of FESEM, AFM, XRD, XPS, Hall effect measurement, and UV-vis spectrophotometry.

Delivered by Publishing Technology to: Kyung Hee University
IP: 115.145.129.113 On: Wed, 01 Oct 2014 06:03:27
Copyright: American Scientific Publishers

For sample B, FESEM and AFM results showed a uniform surface morphology of the ITO thin films compared to that of other samples. As a result, sample B, which was heat-treated at 550 °C, exhibited superb resistivity ($\sim 9.90 \times 10^{-3}$ Ω·cm), excellent transmittance (~92.08%), and superb FOM (105.6×10^{-5} Ω^{-1}). The performance enhancement of sample B may be explained by the high densification of the ITO surface owing to spin-coating resulting in high mobility, and the formation of uniform ITO thin films using electrospray. These results indicate that the ITO thin films fabricated using electrospray and spin-coating may be a potential approach for fabricating highly efficient, solution-based TCOs.

Acknowledgments: This work was supported by Grant No. 10041161 from the Ministry of Knowledge Economy (MKE) and the Fundamental R&D Program for Core Technology of Materials funded by the Ministry of Knowledge Economy, Republic of Korea.

References and Notes

1. C. G. Granqvist and A. Hultaker, *Thin Solid Films* 411, 1 (**2002**).
2. N. R. Armstrong, P. A. Veneman, E. Ratcliff, D. Placencia, and M. Brumbach, *Accounts. Chem. Res.* 42, 1748 (**2009**).
3. H. Kim, C. M. Gilmore, A. Piqué, J. S. Horwitz, H. Mattoussi, H. Murata, Z. H. Kafafi, and D. B. Chrisey, *J. Appl. Phys.* 86, 6451 (**1999**).
4. H. Yumoto, T. Inoue, S. J. Li, T. Sako, and K. Nishiyama, *Thin Solid Films* 345, 38 (**1999**).
5. G. Sberveglieri, P. Benussi, G. Coccoli, S. Groppelli, and P. Nelli, *Thin Solid Films* 186, 349 (**1990**).
6. S. Bhagwat and R. P. Howson, *Surf. Coat. Tech.* 111, 163 (**1999**).
7. D. C. Paine, T. Whitson, D. Janiac, R. Beresford, C. O. Yang, and B. Lewis, *J. Appl. Phys.* 85, 8445 (**1999**).
8. T. Maruyama and K. Fukui, *J. Appl. Phys.* 70, 3848 (**1991**).
9. A. V. Moholkar, S. M. Pawar, K. Y. Rajpure, V. Ganesan, and C. H. Bhosale, *J. Alloy. Compd.* 464, 387 (**2008**).
10. M.-S. Hwang, B.-Y. Jeong, J. H. Moon, S.-K. Chun, and J. H. Kim, *Mater. Sci. Eng., B* 176, 1128 (**2011**).
11. C.-C. Ting, W.-L. Cheng, and G.-C. Lin, *Thin Solid Films* 519, 4286 (**2011**).
12. P. R. Chiarot, P. Sullivan, and R. B. Mrad, *J. Microelectromech. S.* 20, 1241 (**2011**).
13. J.-L. Huang, Y. Pan, J. Y. Chang, and B.-S. Yau, *Surf. Coat. Tech.* 184, 188 (**2004**).
14. S. H. Yu, L. H. Ding, C. Xue, L. Chen, and W. F. Zhang, *J. Non-Cryst. Solids* 358, 3137 (**2012**).
15. C.-H. Liang, S.-C. Chen, X. Qi, C.-S. Chen, and C.-C. Yang, *Thin Solid Films* 519, 345 (**2010**).
16. K. Daoudi, C. S. Sandu, V. S. Teodorescu, C. Ghica, B. Canut, M. G. Blanchin, J. A. Roger, M. Oueslati, and B. Bessa, *Cryst. Eng.* 5, 187 (**2002**).
17. S. Song, T. Yang, J. Liu, Y. Xin, Y. Li, and S. Han, *Appl. Surf. Sci.* 257, 7061 (**2011**).
18. S.-J. Hong and J.-I. Han, *Curr. Appl. Phys.* 6S1, e206 (**2006**).
19. J. F. Moulder, W. F. Stickle, P. E. Sobol, and K. D. Bomben, Handbook of X-ray Photoelectron Spectroscopy, Physical Electronics, Inc., Eden Pairie, (**1995**), pp. 124–127.
20. Y. Igasaki and H. Saito, *Thin Solid Films* 199, 223 (**1991**).
21. J. Liu, A. W. Hains, J. D. Servaites, M. A. Ratner, and T. J. Marks, *Chem. Mater.* 21, 5258 (**2009**).
22. G. Haacke, *J. Appl. Phys.* 47, 4086 (**1976**).

Delivered by Publishing Technology to: Sung Kyun Kwan University
IP: 115.145.129.113 On: Wed, 01 Oct 2014 02:23:27
Copyright: American Scientific Publishers

Received: 9 April 2013. Accepted: 3 December 2013.